(Received 28 July 2025, Accepted 1 September 2025, Scheduled 8 September 2025)

A Miniaturized CPW-Fed Flexible Antenna Sensor for Implantable Breast Tumour Detection with Wireless Powering

Samuelraj Chrysolite*, Suresh Dhanu Shree, and Guruvayurappan Venika

Biomedical Engineering, Karunya University, Coimbatore, India

ABSTRACT: Early detection of breast tumor is crucial for reducing the likelihood of mastectomy. To monitor the dielectric changes in breast tissue caused by the formation of tumorous cells, a novel biocompatible implantable antenna sensor is proposed. This flexible implant, measuring just 5 mm × 5 mm × 0.25 mm, operates in the ISM band at 2.45 GHz for real-time breast tumor detection. It is wirelessly powered via Wireless Power Transfer (WPT) operating in the mid-band range of 1.2–1.4 GHz. The antenna achieves an ultra-compact volume of 12.5 mm^3 through closed-loop structures and meandered strips that enhance radiation efficiency. Inside abnormal breast tissue with a relative permittivity (ε_r) of 52.7, the antenna demonstrates a reflection coefficient of −17 dB and offers a −10 dB bandwidth of 330 MHz. The sensor is activated when the tissue permittivity rises above 15, achieving a maximum gain of −10 dBi. The antenna has been fabricated, and the simulated results have been validated in-vivo. This design enables proactive detection of tumor cell formation within breast tissue, allowing treatment before it spreads. It is particularly suitable for individuals with a genetic predisposition to breast tumor, offering continuous monitoring for early intervention.

1. INTRODUCTION

Advances in wireless, batteryless implantable electronics have enabled continuous physiological monitoring, opening new possibilities for cancer surveillance [1]. Early detection of malignant changes is critical for timely therapeutic intervention and improved survival outcomes [2], particularly in organs with high cancer susceptibility such as the breasts, skin, lungs, colon, bones, and prostate [3]. Breast cancer remains one of the most common malignancies worldwide [4], with genetic predisposition significantly contributing to early onset [5]. In aggressive subtypes like triple-negative breast cancer, tumor cells may double within a matter of weeks, underscoring the need for proactive detection strategies. While current clinical tools such as Magnetic Resonance Imaging (MRI), ultrasound, and mammography are widely used [6–8], they present limitations including high cost, exposure to ionizing radiation, and operator dependency [9]. Microwave-based sensing offers a promising alternative due to the marked differences in dielectric properties between healthy and cancerous tissues [10]. Wearable antenna arrays have been investigated for noninvasive breast tumor detection [11–16], yet challenges persist in ensuring comfort, compliance with Specific Absorption Rate (SAR) safety limits, and maintaining detection accuracy during patient movement. Implantable antennas address these shortcomings by enabling stable in-vivo measurements but must overcome hurdles in miniaturization, biocompatibility, and efficient wireless power transfer [17–19]. Recent studies have demonstrated the potential of resonator-based architectures for tracking pathological changes by monitoring resonant frequency shifts [17], while others have leveraged metamaterials and artificial magnetic conductors to enhance detection sensitivity and reduce device size [7, 10, 11]. Wireless power transfer (WPT) systems, including mid-band inductive links [2, 3, 14, 15, 17, 18], have been developed to eliminate battery dependency and enable long-term operation in vivo. Such systems must be designed to operate efficiently through lossy biological media while adhering to SAR safety standards [21].

In this context, we propose a miniaturized coplanar waveguide (CPW)-fed flexible implantable antenna sensor for proactive breast tumor detection. The sensor operates at 2.45 GHz in the Industrial, Scientific, and Medical (ISM) band for real-time monitoring and is powered wirelessly in the 1.2–1.4 GHz mid-band range, eliminating the need for batteries. By employing multiple meandered closed-loop structures, the design achieves enhanced radiation efficiency, extended sensing range, and high compactness while preserving biocompatibility. Importantly, the device remains dormant under normal tissue conditions and activates when local dielectric permittivity exceeds a malignant threshold, enabling early warning before tumor growth reaches clinically significant stages. This approach provides a pathway toward continuous, minimally invasive breast cancer monitoring, particularly benefiting individuals at elevated genetic risk, while reducing the likelihood of delayed diagnosis and the need for extensive treatment.

2. ANTENNA SENSOR DESIGN

The proposed antenna sensor features a compact size of $5 \times 5 \times 0.25\,mm^3$, with the radiating element printed on a flexible RT Duroid 6010 substrate (dielectric constant $\varepsilon_r = 10.2$) having a thickness of 0.25 mm. To improve biocompatibility,

* Corresponding author: Samuelraj Chrysolite (samuelraj@karunya.edu).

the radiating patch is encapsulated with a flexible superstrate — also made of RT Duroid 6010 with a thickness of 0.25 mm — preventing direct contact with living tissues after implantation. The antenna utilizes an edge-fed configuration, with the feed positioned at the center of the right-hand side edge. A coplanar feed structure is used to reduce feed-point radiation and improve bandwidth, enhancing breast tumor detection. The complete structural layout along with the design parameters is illustrated in Figure 1, and the detailed parameter values are provided in Table 1. A 50 Ω SMA connector is used to interface the antenna sensor with the external system. The antenna sensor was fabricated via subtractive manufacturing (Micro-Etching) on RT/Duroid® 6010, with a biocompatible encapsulating superstrate to minimize tissue reaction and ensure long-term implantation stability.

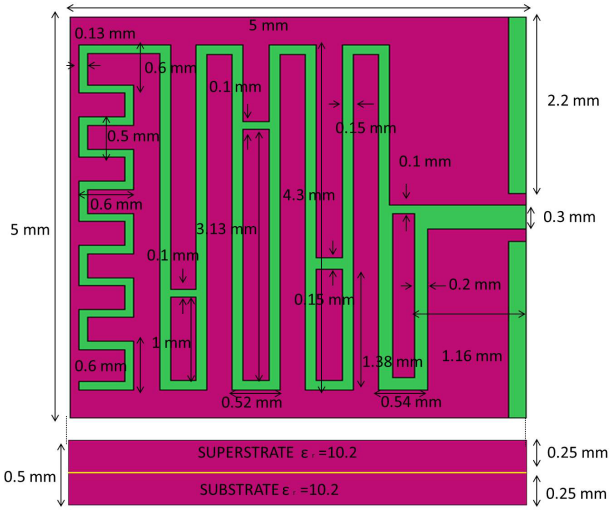

FIGURE 1. Structural design of the proposed antenna sensor.

TABLE 1. Parameters of proposed antenna sensor.

Parameters	Values (mm)	Parameters	Values (mm)
Substrate Width	5	Loop 2 width	0.15
Substrate Depth	5	Loop 3,4 width	0.1
Substrate Height	0.25	Initial Loop Depth	0.2
Superstrate Height	0.25	Middle Loop Depth	0.15
Ground Depth (G1,G2)	2.2	Later Loop Depth	0.13
Ground Width	0.2	Feed Depth	1.16
Feed Width	0.3	Loop 1 width	0.1

2.1. Breast Simulation Model

Most healthy breast tissue is composed of fat. However, when cells turn tumorous, both the dielectric permittivity and tissue density increase, making them comparable to those of muscle tissue. To replicate the environment of tumorous breast tissue, a muscle-skin layer phantom was modeled using Altair Feko v.2020. This simulated phantom includes layers representing muscle and skin tissues, as illustrated in Figure 2. The skin layer was assigned a height of 2.2 mm, while the muscle layer was set at 30 mm. Table 2 gives the associated relative permittivity and loss tangent values.

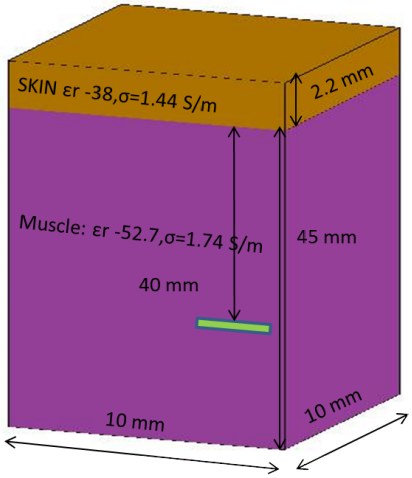

FIGURE 2. Implant environment.

TABLE 2. Parameters of breast simulation model.

Tissue	ε_r @ 2.45 GHz	tan δ @ 2.45 GHz(S/m)
Muscle	52.7	1.74
Skin	38	1.44

2.2. Sensing Performance

The sensing performance of the antenna sensor is influenced by the implantation environment, specifically the muscle tissues, which act as the surrounding dielectric medium [18]. With its parallel combination of capacitance and inductance (C_0 and L_0), the implanted antenna sensor operates similarly to a standard monopole antenna. The surrounding muscle and tissue environment introduces an additional capacitance, denoted as C_t. The closed-loop structures, illustrated in Figure 1, generate parallel inductances L_1, L_2, L_3, and L_4, which help tune the antenna's resonant frequency to 2.45 GHz (within the ISM band), effectively compensating for the combined capacitances C_0 and C_t caused by the antenna sensor and surrounding tissues. As the tissue becomes tumorous, its relative permittivity changes, leading to a variation in C_t. Figure 3 shows the complete equivalent circuit model.

In the body environment, the implantable antenna sensor's total capacitance is determined by $C = C_0 + C_t$, where C_0 is the inherent capacitance of the antenna sensor, and C_t is the capacitance due to the surrounding tissues. The antenna sensor's sensitivity can be enhanced by incorporating closed inductive loops. Typically, the resonant frequency is calculated using Equation (1).

$$f_0 = \frac{1}{2\pi\sqrt{L_0 C}} \tag{1}$$

When inductive loops are introduced, the total inductance becomes a combination of L_0 and L_c, where $L_c = L_1 + L_2 +$

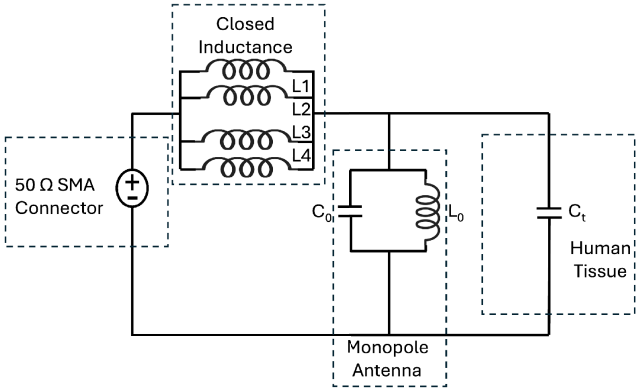

FIGURE 3. Equivalent circuit of breast tumor sensor in implant surroundings.

$L_3 + L_4$. The modified expression for resonant frequency is given in Equation (2).

$$f = \frac{1}{2\pi\sqrt{\frac{L_c L_0}{L_c + L_0} C}} \tag{2}$$

As the surrounding tissue becomes tumorous, the permittivity changes, which alters the value of C_t and, consequently, the total capacitance C. The resulting change in resonant frequency due to this variation in C can be evaluated by *partially differentiating* Equations (1) and (2) with respect to capacitance, as shown in Equations (3) and (4).

$$\frac{\partial f_0}{\partial C} = -\frac{1}{4\pi}\sqrt{\frac{1}{L_0}} C^{-\frac{3}{2}} \tag{3}$$

$$\frac{\partial f}{\partial C} = -\frac{1}{4\pi}\sqrt{\frac{L_c + L_0}{L_c L_0}} C^{-\frac{3}{2}} \tag{4}$$

Rearranging Equation (4) in terms of Equation (3) gives Equation (5) which is the change in resonant frequency with respect to the change in capacitance C.

$$\frac{\partial f}{\partial C} = \sqrt{1 + \frac{L_0}{L_c}} \frac{\partial f_0}{\partial C} \tag{5}$$

3. OPTIMIZATION OF PROPOSED ANTENNA

3.1. Inductance Loops

In order to guarantee impedance matching with the 50 Ω SMA connector feed, the structural design has been optimized. This optimization process is illustrated in Figures 4(a) to (e), where the number of inductive loops is progressively increased. The resonant frequency is tuned to 2.45 GHz by distributing the current flow by splitting the current flow across each S-shaped monopole segment incorporating loops. The S-shaped monopole is widened at the feed point and gradually tapered toward the radiating end. The resulting improvement in current distribution with the addition of loops is clearly depicted in Figure 4.

The addition of inductive loops shifted the resonance frequency from 2.16 GHz to 2.44 GHz with minimal impact on the reflection coefficient, as illustrated in Figure 5. Furthermore, the impedance bandwidth improved by 10%, increasing from 400 MHz to 462 MHz, effectively covering a frequency range from 2.25 GHz to 2.7 GHz within the −10 dB reflection bandwidth.

3.2. Ground Widths

Among the different designs, the configuration with four inductive loops demonstrated superior performance and was selected for further bandwidth enhancement. This was achieved by reducing the ground plane width from 1 mm to 0.2 mm in 0.4 mm steps, effectively minimizing stray capacitances. As a result, an additional 200 kHz improvement in impedance bandwidth was obtained at a ground width of 0.2 mm. The reflection coefficient for various ground widths is shown in Figure 6. Therefore, the final design chosen for further sensing performance analysis features four inductive loops with varying widths and a ground plane width of 0.2 mm.

4. RESULTS AND DISCUSSION

4.1. Simulation Results

The relative permittivity of healthy breast tissue is approximately 5, corresponding to fatty tissue, while tumorous breast tissue exhibits a much higher relative permittivity of around 52, similar to muscle tissue [20]. As the permittivity of the tissue increases due to tumor development, a noticeable shift in the antenna's resonant frequency occurs, as illustrated in Figure 7. Specifically, the resonant frequency decreases with the rise in tissue permittivity. The proposed antenna sensor shows poor S_{11} performance when being simulated in an air environment ($\varepsilon_r = 1$), representing conditions outside the body, as shown in Figure 7. Resonance shifting begins once the antenna sensor is in contact with tumorous breast tissue and continues as the relative permittivity increases, indicating progressive tumor growth. When the relative permittivity of the breast tissue is 5.28 (typical for normal internal breast tissue), the antenna sensor does not radiate. However, it begins sensing tumorous changes once the permittivity exceeds $\varepsilon_r = 15$, signalling the early stages of tumor. The $\varepsilon_r > 15$ threshold is determined by the average characteristics of malignant tissue; however, permittivity can vary with age, tissue type, or physiological conditions such as breastfeeding. Despite these fluctuations, the antenna's broad bandwidth and linear response guarantee efficient identification. Additionally, subject-specific calibration can improve accuracy. However, the sensor does not differentiate between malignant and benign lesions, as conditions like fibroadenomas or inflammation may also increase permittivity. Thus, it serves as an early warning system, prompting further imaging or biopsy for definitive diagnosis. As the permittivity increases to around 25, representing larger tumor, the resonant frequency continues to shift further left. Detecting tumor progression before permittivity reaches this level enables early diagnosis and may reduce the extent of required treatment. Breast tumors are considered advanced when permittivity ranges be-

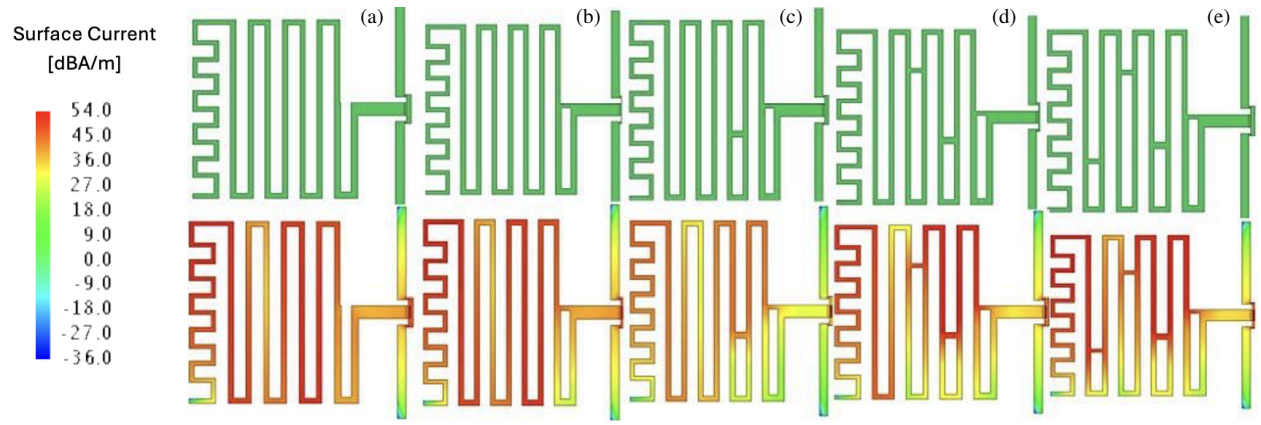

FIGURE 4. Current distribution of antenna sensor with inductance loops (comparison). (a) No loop. (b) One loop. (c) Two loops. (d) Three loops. (e) Four loops.

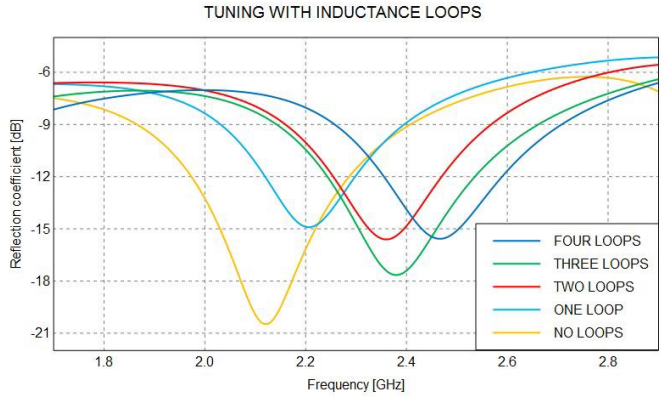

FIGURE 5. Reflection coefficient for different number of inductance loops.

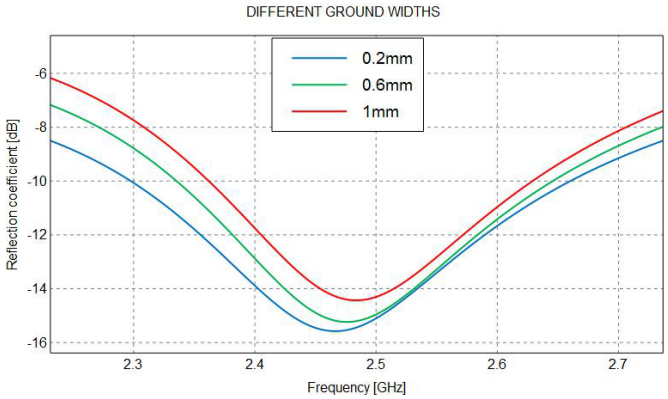

FIGURE 6. Reflection coefficient for different ground widths.

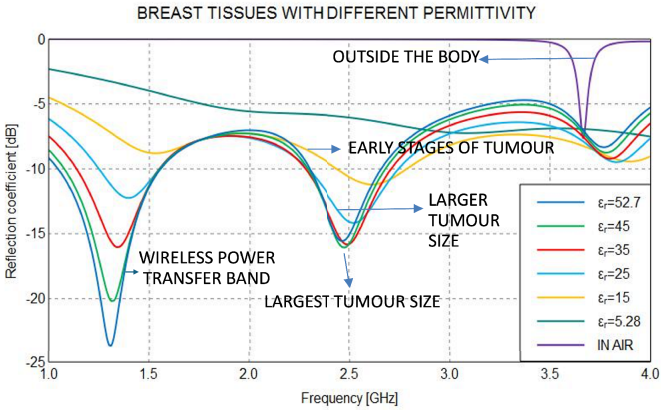

FIGURE 7. Reflection coefficient for different relative permittivity of breast tissues.

tween 35 and 50. Early detection using the proposed antenna sensor can help avoid reaching this critical stage. The wide reflection bandwidth of 512 MHz (from 2.25 GHz to 2.75 GHz at -10 dB) enables effective early detection of tumorous tissue growth. The key innovation of the proposed antenna sensor lies in its ability to proactively detect breast tumor in its early stages, which is vital in reducing the risk of mastectomy in malignant cases. It is recommended that individuals with the implant consult a doctor every ten days to monitor any potential development of tumorous tissues before tumor size significantly increases.

Antenna sensor is capable of being wirelessly powered through wireless power transfer. This power transfer is carried out at a mid-band frequency of 1.4 GHz, which is suitable for the proposed antenna design. At this frequency, a reflection coefficient of -23 dB is achieved, indicating efficient power transfer capability. Notably, this frequency band becomes active only when the surrounding tissue turns malignant, triggering the antenna sensor to begin transmitting at 2.45 GHz. For effective wireless power delivery, a high-gain transmitter antenna at 1.4 GHz can be placed near the patient to power the implantable sensor. The proposed antenna sensor integrates a Wireless Power Transfer (WPT) module operating at 1.2–1.4 GHz, enabling battery-free operation and long-term in-vivo deployment. This mid-band powering system ensures stable energy delivery without compromising tissue safety, supporting continuous tumor monitoring.

The shift in resonant frequency is also represented on a linear graph with curve fitting, as shown in Figure 8. The resulting curve follows the equation $f = 2.4587 - 0.00016\varepsilon_r$, where f is the resonant frequency. This equation can be used to estimate the relative permittivity ε_r of the tumorous tissue when the resonant frequency is known.

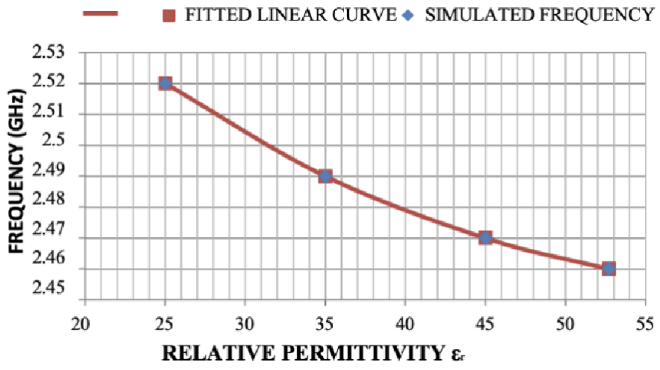

FIGURE 8. Linear fitting curve resonance frequency vs relative permittivity of breast tissue.

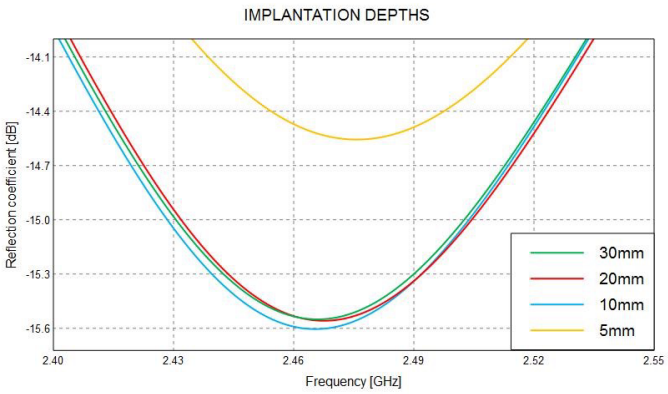

FIGURE 9. Reflection coefficient at various implantation depths.

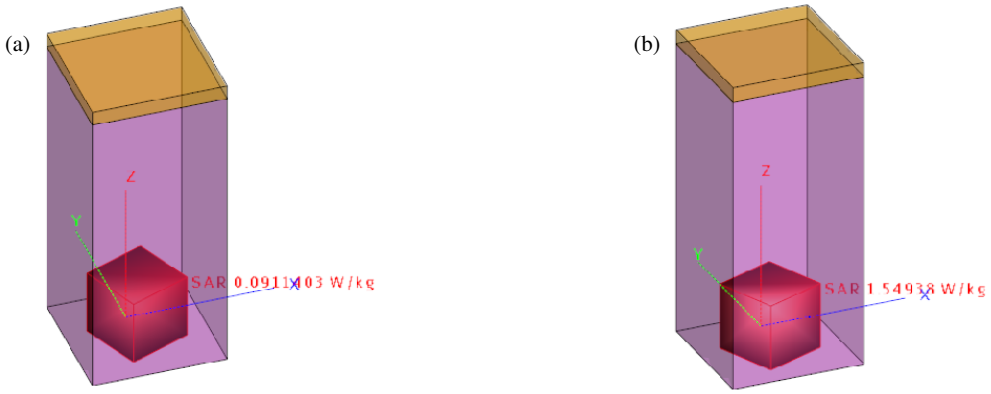

FIGURE 10. Spatial peak SAR for normal and malignant breast tissues (input power-5 mW). (a) Spatial peak SAR for normal breast. (b) Spatial peak SAR for malignant breast.

The sensitivity of the implanted antenna sensor to its surrounding environment was evaluated by analysing its performance at various implantation depths within the muscle layer. Depths up to 30 mm were studied to ensure that no significant shift in the resonant frequency occurred. As shown in Figure 9, the resonant frequency remains consistent across different implantation depths.

Surrounding tissues, including muscle, absorb the emitted radiation. The quantity of radiation absorbed by the muscles and tissues can be measured by a measurement called Specific Absorption Rate (SAR), which is computed by (6). According to IEEE standard C95.1-1999, SAR should not exceed 1.6 W/kg per 1 g of tissue of the human body [21]. Spatial peak (1 gram) SAR values of 0.091 W/kg and 1.54 W/kg are obtained for normal breast tissue and malignant breast tissue, respectively, at an input power of 5 mW, as illustrated in Figures 10(a) and (b). The system operates at just 5 mW, and SAR values remain within the IEEE safety limit of 1.6 W/kg. No short-term biological effects are expected at 2.45 GHz and 1.2–1.4 GHz, although the long-term effects of radio frequency (RF) exposure warrant further in-vivo investigation.

$$\text{SAR} = \frac{\sigma E_{\text{RMS}}^2}{\rho} \tag{6}$$

SAR = Specific absorption rate

σ = Conductivity of various human tissues

E_{rms} = Root-mean-square (RMS) of electric intensity of the body

ρ = Density of human tissue.

Over time, the performance of implantable antennas may be influenced by physiological factors such as tissue encapsulation, fluid absorption, and dielectric property changes. These factors can lead to minor detuning in resonant frequency or reflection characteristics. However, the wide -10 dB bandwidth of 512 MHz ensures stable operation despite such variations. The use of RT Duroid 6010 as a biocompatible encapsulant offers excellent mechanical and dielectric stability, preserving both structural integrity and sensor performance over extended periods in vivo.

4.2. Experimental Setup and Validation

Measurements of the radiation gain and reflection coefficient were conducted during manufacturing in order to validate the simulated results and confirm the functionality of the suggested antenna sensor prototype. The fabricated antenna sensor can be seen in Figure 11(a). As seen in Figure 11(b), a coplanar feed is

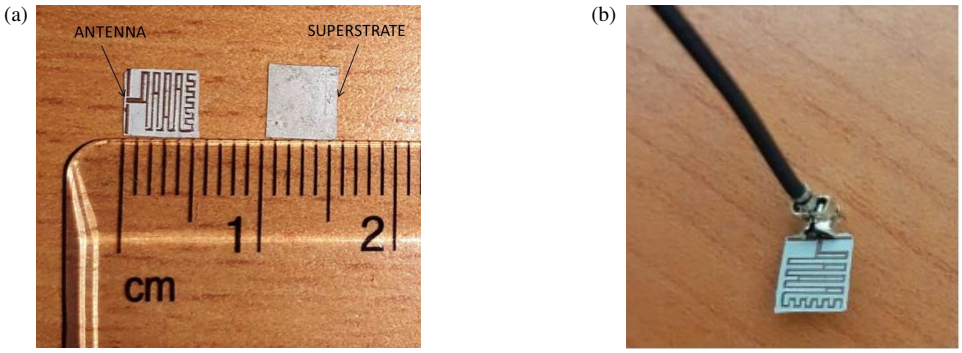

FIGURE 11. Fabricated antenna sensor. (a) Measurement of antenna sensor. (b) Antenna sensor with coplanar feed.

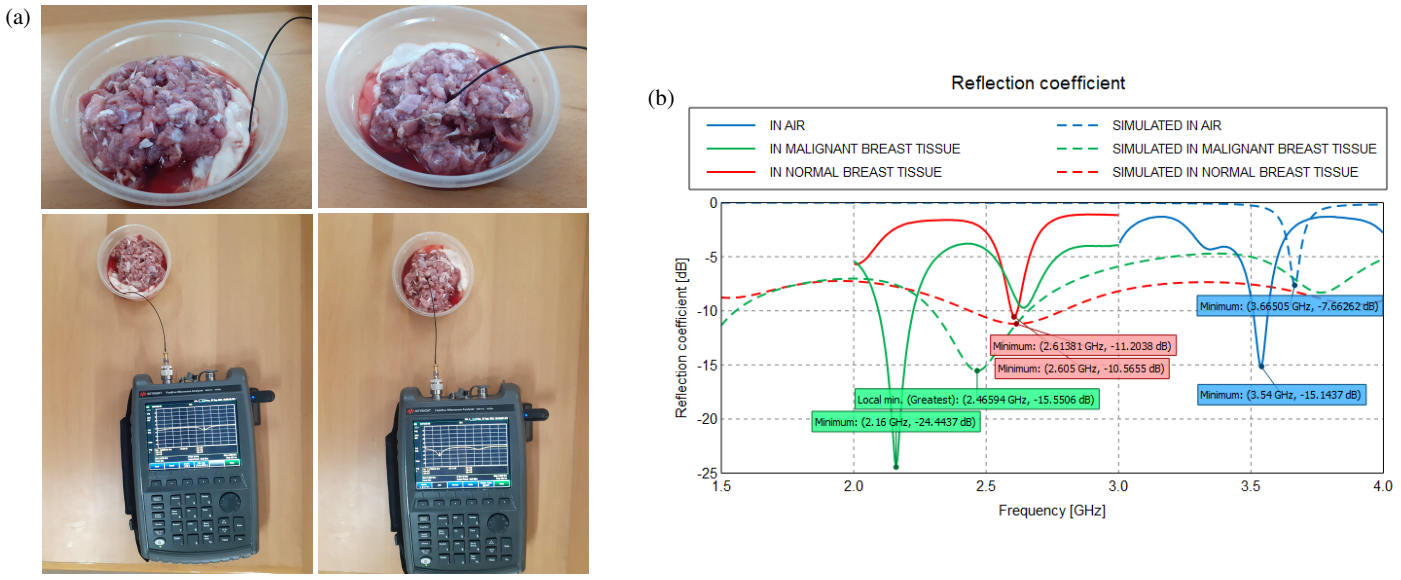

FIGURE 12. In-vivo setup and measurement with pork muscle/fat. (a) Experimental setup with VNA. (b) Reflection coefficient — Comparison for normal breast tissue vs tumorous breast tissue.

connected to the suggested antenna sensor, and vector network analyser (VNA) is used to verify the findings.

For testing, the manufactured antenna sensor was positioned inside pork muscle, which resembles malignant breast tissue, and pork fat, which represents normal breast tissue. The antenna sensor prototype was fabricated using subtractive manufacturing (Micro-Etching) on an RT/Duroid® 6010 substrate, ensuring accurate dimensional control and consistent electrical performance for experimental validation. It was connected to a vector network analyzer. The antenna sensor was positioned 30 mm deep within the pig muscle or fat. Figure 12(a) depicts the experimental setup for inserting the suggested antenna sensor into the pork muscle or fat. Figure 12(b) compares the simulated results with the resonant frequency shift that occurs when the suggested antenna sensor is inserted inside the pork muscle and fat. One hundred grams of pork muscle, which mimics malignant tissue, was used in the experiment. However, the suggested antenna sensor detects even when the malignant tissue weighs less than 10 grams (1000 mm^3). The micro-antenna detects dielectric changes only in its immediate vicinity and does not provide spatial localization. Tumors smaller than 5 mm can be detected if they are present near the implant site. Detecting and localizing tumors over a broader area would require a sensor array or external scanning setup. The resonant frequency shifts proportionally with the size of the cancerous tissue. The results indicate that the resonant frequency of the suggested antenna sensor is also influenced by the size of the malignant tumor. Consequently, a deviation between the measured value of 2.15 GHz and the simulated value of 2.45 GHz is acceptable.

The simulated and measured radiation patterns (normal and cancerous) are compared as shown in Figure 13. Peak gains of -38.5 dBi for normal tissue and -42.5 dBi for malignant tissue were recorded. The low gains (-38.5 to -42.5 dBi) are expected in lossy biological tissues due to absorption and dielectric losses. The sensor is optimized for short-range telemetry to a nearby external reader, with range improvements possible via high-sensitivity receivers or high-gain reader antennas. The gain value is sufficient for sensing the tumor development inside the breast.

A comparison between existing implantable antennas with proposed antenna sensor is listed in Table 3.

TABLE 3. Comparison with current knowledge in implantable antennas.

Citation Author (Year)	Fr Band	ε_r	Radiating Patch	Patch Size [mm]	S_{11} [dB]	Gain [dBi]	SAR Limit [W/kg] I g of tissue
Nabeel Ahmed Malik (2020)	240 MHz	10.2	Copper cladding	$4 \times 4 \times 0.3$	-21	3.22	589
Zhiwei Song (2024)	0.61–1.51 GHz	N/A	N/A	$7 \times 6.5 \times 0.377$	-22	-28.8	652.3
Singh et al. (2021)	402–405 MHz	4.4	Inset-fed microstrip	15×15	-26.57	N/A	N/A
Chaurasia et al. (2024)	3.5–11.7 GHz	N/A	UWB Patch Array	N/A (7-element)	-50.83 @ 8 GHz	8.84	N/A
Mary Neebha (2020)	5.8 GHz	3.5	AMC based Monopole	$4.6 \times 7.6 \times 0.15$	-41	1.638	0.8350
Wei Wang (2021)	2.45 GHz	10.2	S shaped Meandered	$5 \times 5 \times 0.6$	-40	-17.9	1.58
Leena & Kumar (2025)	2.45 GHz	N/A	Circular Patch + AMC	N/A	-10.0 to -10.3	N/A	0.139
Pawar et al. (2023)	2.35–2.55 GHz	2.2	CPW-fed truncated patch	$21 \times 13.5 \times 0.254$	-22 to -10	N/A	0.78
Proposed Work	**2.1–3.1 GHz**	**10.2**	**Multiple meandered loops**	$\mathbf{5 \times 5 \times 0.5}$	$\mathbf{-17}$	$\mathbf{-38.5}$	**1.01**

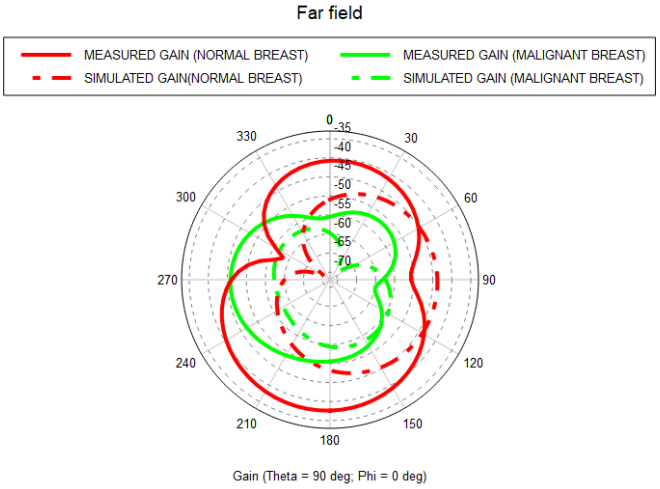

FIGURE 13. Simulated and measured gains in normal and tumorous breasts.

5. CONCLUSION

The proposed antenna sensor was constructed, and its radiation properties were confirmed. To improve the sensitivity and reflection bandwidth for proactive tumorous cell detection, closed loops were added. The ground width was decreased in the coplanar structure to lessen side lobes and, consequently, power loss. Using the antenna sensor, the pathogenic changes in the breast tissues can be identified. As a result, it can be utilized for non-contact monitoring of cancer patients who are at risk for the disease or those who have already undergone therapy. Additionally, it offers wireless power transfer and charging via a nearby transmitter at the residence or medical facility. Future work can explore optimized monitoring environments for clinical deployment. User centric parameters like biocompatibility and patient comfort can also be added. Further clinical translation and real world challenges can be pondered upon. The analysis of interference mitigation from other devices operating on the same frequency is also possible.

REFERENCES

[1] Kim, H., B. Rigo, G. Wong, Y. J. Lee, and W.-H. Yeo, "Advances in wireless, batteryless, implantable electronics for real-time, continuous physiological monitoring," *Nano-Micro Letters*, Vol. 16, No. 1, 52, 2024.

[2] Nithiyanandam, V. and V. Sampath, "Approach-based analysis on wireless power transmission for bio-implantable devices," *Applied Sciences*, Vol. 13, No. 1, 415, 2023.

[3] Mahmud, S., A. Nezaratizadeh, A. B. Satriya, Y.-K. Yoon, J. S. Ho, and A. Khalifa, "Harnessing metamaterials for efficient wireless power transfer for implantable medical devices," *Bioelectronic Medicine*, Vol. 10, No. 1, 7, 2024.

[4] Khaleghi, A., A. Hasanvand, and I. Balasingham, "Design and implementation of a hybrid wireless power and communication system for medical implants," in *2023 IEEE MTT-S International Microwave Biomedical Conference (IMBioC)*, 52–54, Leuven, Belgium, 2023.

[5] Wang, W., Z. Yu, Y. Zou, J. E. Woods, P. Chari, Y. Su, J. T. Robinson, and K. Yang, "Omnidirectional wireless power transfer for millimetric magnetoelectric biomedical implants," *IEEE Journal of Solid-State Circuits*, Vol. 59, No. 11, 3599–3611, 2024.

[6] Omi, A. I., A. Jiang, and B. Chatterjee, "A systematic method for optimum biomedical wireless power transfer using inductive links in area-constrained implants," *ArXiv Preprint ArXiv:2501.08766*, 2025.

[7] Leena, V. and N. Kumar, "Quasi crystal based circular patch antenna with artificial magnetic conductor for breast cancer detection," *ArXiv Preprint ArXiv:2502.16269*, 2025.

[8] Huda, S. M. A., M. Y. Arafat, and S. Moh, "Wireless power transfer in wirelessly powered sensor networks: A review of recent progress," *Sensors*, Vol. 22, No. 8, 2952, 2022.

[9] Zhang, J., R. Das, J. Zhao, N. Mirzai, J. Mercer, and H. Heidari, "Battery-free and wireless technologies for cardiovascular implantable medical devices," *Advanced Materials Technologies*, Vol. 7, No. 6, 2101086, 2022.

[10] Hamza, M. N., M. T. Islam, and S. Koziel, "Advanced sensor for non-invasive breast cancer and brain cancer diagnosis using antenna array with metamaterial-based AMC," *Engineering Science and Technology, An International Journal*, Vol. 56, 101779, 2024.

[11] Mohan, A. and N. Kumar, "Implantable antennas for biomedical applications: A systematic review," *BioMedical Engineering OnLine*, Vol. 23, No. 1, 87, 2024.

[12] Smida, J., M. K. Azizi, A. S. C. Bose, and M. I. Waly, "A compact implantable multiple-input-multiple-output antenna for biotelemetry and sensing applications," *Sensors*, Vol. 25, No. 11, 3323, 2025.

[13] Jasim, M., A. J. A. Al-Gburi, M. Hanif, Z. A. Dayo, M. M. Ismail, and Z. Zakaria, "An extensive review on implantable antennas for biomedical applications: Health considerations, geometries, fabrication techniques, and challenges," *Alexandria Engineering Journal*, Vol. 112, 110–139, 2025.

[14] Hazrati Marangalou, A., M. Gonzalez, N. Reppucci, and U. Guler, "A design review for biomedical wireless power transfer systems with a three-coil inductive link through a case study for NICU applications," *Electronics*, Vol. 13, No. 19, 3947, 2024.

[15] Shaw, T., B. Mandal, G. Samanta, T. Voigt, D. Mitra, and R. Augustine, "Rotation insensitive implantable wireless power transfer system for medical devices using metamaterial-polarization converter," *Scientific Reports*, Vol. 14, No. 1, 19688, 2024.

[16] Rana, M. M., M. A. Islam, and I. M. Mehedi, "Dual-band implantable antenna loaded with patch slots for wireless biotelemetry systems," *Progress In Electromagnetics Research C*, Vol. 141, 151–162, 2024.

[17] Yan, X., J. Yao, W. Chen, and Y. Song, "Wireless power transfer system for cardiac pacemakers based on multi-coil series magnetic integration," *Progress In Electromagnetics Research C*, Vol. 143, 87–98, 2024.

[18] Fernandez-Munoz, M., M. Missous, M. Sadeghi, P. L. Lopez-Espi, R. Sanchez-Montero, J. A. Martinez-Rojas, and E. Diez-Jimenez, "Fully integrated miniaturized wireless power transfer rectenna for medical applications tested inside biological tissues," *Electronics*, Vol. 13, No. 16, 3159, 2024.

[19] Al-Gburi, R. M., M. Alibakhshikenari, B. S. Virdee, T. M. Hameed, D. Mariyanayagam, S. Fernando, I. Lubangakene, Y. Tang, S. U. Khan, and T. A. Elwi, "Microwave-based breast cancer detection using a high-gain Vivaldi antenna and metasurface neural network approach for medical diagnostics," *Frequenz*, Vol. 79, No. 7–8, 311–325, 2025.

[20] Gabriel, C., S. Gabriel, and Y. E. Corthout, "The dielectric properties of biological tissues: I. Literature survey," *Physics in Medicine & Biology*, Vol. 41, No. 11, 2231, 1996.

[21] Safety, Electromagnetic, IEEE C95.7/DRAFT, 2005.